Turbulence suppression in channel flows by small amplitude transverse wall oscillations

Mihailo R. Jovanović[a)]
Department of Electrical and Computer Engineering, University of Minnesota, Minneapolis, Minnesota 55455, USA

(Received 7 August 2007; accepted 8 November 2007; published online 11 January 2008)

We model and analyze the influence of small amplitude transverse wall oscillations on the evolution of velocity perturbations in channel flows. We quantify the effect of stochastic outside disturbances on velocity perturbation energy and develop a framework for the optimal selection of transverse oscillation parameters for turbulence suppression. A perturbation analysis is used to demonstrate that depending on the wall oscillation frequency the energy of velocity perturbations can be increased or decreased compared to the uncontrolled flow. Our results elucidate the capability of properly designed oscillations to reduce receptivity of the linearized Navier-Stokes equations to stochastic disturbances, which entails decreased levels of variance in wall-bounded shear flows.
 [DOI: 10.1063/1.2824401]

I. INTRODUCTION

Skin-friction drag reduction by sensorless mechanisms is a promising technology for implementation, as it represents a much simpler alternative to feedback flow control with wall-mounted arrays of sensors and actuators. Examples of sensorless strategies include transverse wall oscillations, control of conductive fluids using the Lorentz force, and wall geometry deformation such as riblets. Each of these strategies is characterized by the absence of sensing capabilities. In other words, control is implemented without measurement of the relevant flow quantities and disturbances. Rather, the dynamical properties of the underlying system are changed by either modifying geometry (riblets) or nominal velocity (wall oscillations and Lorentz forces). Although several numerical and experimental investigations indicate that *properly designed* sensorless strategies can lead to a significant drag reduction, an obstacle to fully utilize these approaches is the absence of a theoretical framework for their design and optimization. This lack of analytical tools greatly impedes the design and optimization of sensorless schemes as well as their extension to different flow regimes.

Skin-friction drag reduction by means of transverse oscillations was first explored in Ref. 1. The direct numerical simulations of a turbulent channel flow subject to either a spanwise oscillatory wall motion or an oscillatory spanwise body force showed that a substantial drag reduction (up to 40%) can be achieved for certain values of oscillation frequency. The attenuation of velocity fluctuations (up to 30%) was also reported. These observations served as a motivation for further numerical and experimental investigations in channel,[2–4] pipe,[5–7] and boundary layer[8–11] flows.

In this paper, we model and analyze the influence of transverse wall oscillations on the evolution of velocity perturbations in *transitional channel flows*. Our results complement previously reported numerical and experimental studies, and furnish a theoretical framework for design of more efficient turbulence suppression strategies. Since the transition in channel flows is not appropriately described by the eigenvalue analysis (see, for example, Refs. 12 and 13), we perform an input-output analysis of stochastically excited linearized Navier-Stokes (NS) equations. Our analysis quantifies the effect of body force fields on velocity perturbations and provides a paradigm for the optimal selection of transverse oscillation parameters for turbulence suppression.

We show that suppression (enhancement) of turbulence by transverse wall oscillations is due to decreased (increased) variance amplification compared to the uncontrolled flow. In other words, the changes in nominal velocity constrain velocity perturbations to experience smaller (for suppression of turbulence) or larger (for enhancement of turbulence) *receptivity* to external disturbances.[14] In the language of control theory, influence of transverse wall oscillations is quantified by the $\mathcal{H}_2$ norm of operator that maps the stochastic outside disturbances (such as free stream turbulence or acoustic waves) to the velocity perturbations. We note that the $\mathcal{H}_2$ norm has an appealing physical interpretation; it represents the *ensemble average energy density* of the statistical steady state.[15,16] The turbulence suppression takes place if the ensemble average energy density is reduced in the presence of control. The system norms were previously employed by Farrell and Ioannou[14] and Kim[17] for evaluation of active flow control strategies. However, to the best of the author's knowledge this approach has not been used for assessing effectiveness of sensorless flow control strategies.

Our approach has strong parallels with the concept of *vibrational control*, where the system's dynamical properties can be changed by introducing zero-mean vibrations into the system's coefficients.[18] Depending on the relationship between the natural modes of the uncontrolled system and the forcing frequency, the vibrational control may have a potential for providing stability of the overall system and for changing its receptivity to external disturbances. For example, it is well known that the inverted pendulum can be

[a)]Electronic mail: mihailo@umn.edu; http://umn.edu/home/mihailo/.

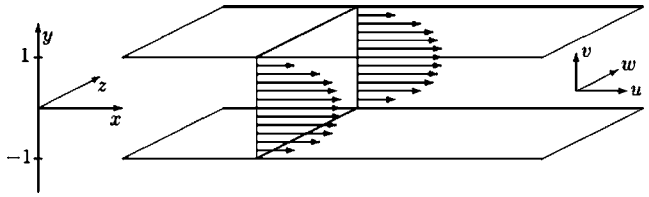

FIG. 1. Three-dimensional channel flow.

stabilized by sensorless means using high frequency oscillations of the suspension point.[18] We show that the principle of vibrational control can be also utilized in systems described by the NS equations, where coefficients multiplying the system's state can have temporal periodicity. The key observation is that there is a potential for changing stability properties and receptivity of the NS equations (in favorable or unfavorable manner) whenever temporal (or spatial) vibrations enter into the system's coefficients.

Our presentation is organized as follows: in Sec. II we determine the nominal velocity of a channel flow subject to transverse wall oscillations, and present a dynamical description of flow fluctuations evolving around this velocity profile. In Sec. III, we introduce a notion of the *frequency response* of linear time-periodic systems and briefly describe a computationally efficient method for determination of the ensemble average energy density in the presence of small amplitude wall oscillations. In Sec. IV, we employ perturbation analysis to identify the oscillation frequency that leads to the largest variance suppression for streamwise constant perturbations. We also provide an explicit dependence of the variance amplification on the Reynolds number R. In Sec. V, we consider the full three-dimensional perturbations in Poiseuille flow with $R=2000$, and compute the ensemble average energy density for oscillation frequency that leads to the largest variance suppression for streamwise constant perturbations. In Sec. VI, we summarize our presentation and give an outlook for future research directions.

II. DYNAMICS OF VELOCITY FLUCTUATIONS

A. Nominal velocity

Consider a flow between two parallel infinite plates with geometry illustrated in Fig. 1. Incompressible flow of a viscous Newtonian fluid satisfies the NS and the continuity equations given in their nondimensional forms by

$$\mathbf{u}_t = -\boldsymbol{\nabla}_{\mathbf{u}}\mathbf{u} - \boldsymbol{\nabla}P + (1/R)\Delta\mathbf{u} + \mathbf{F},$$
$$0 = \boldsymbol{\nabla}\cdot\mathbf{u}, \tag{1}$$

where $\mathbf{u}$ is the velocity vector, P is the pressure, $\mathbf{F}$ is the body force, $\boldsymbol{\nabla}$ is the gradient, $\Delta := \boldsymbol{\nabla}^2$ is the Laplacian, and operator $\boldsymbol{\nabla}_{\mathbf{u}}$ is defined as $\boldsymbol{\nabla}_{\mathbf{u}} := \mathbf{u}\cdot\boldsymbol{\nabla}$. The Reynolds number is defined in terms of maximal nominal velocity $\bar{U}$ and channel half-width δ, $R := \bar{U}\delta/\nu$, where ν denotes the kinematic viscosity.

Let the flow be subject to a transverse oscillation of the lower-wall, and let the nominal body force be equal to zero, $\bar{\mathbf{F}} \equiv 0$. Due to no-slip, the wall oscillation imposes an oscillatory boundary condition on the spanwise component of nominal velocity $\bar{\mathbf{u}} := [U\ V\ W]^T$. If the lower wall oscillates with frequency $\omega_o := 2\pi/T$, the nominal velocity can be determined from Eq. (1) subject to

$$W(-1) := 2\alpha \sin \omega_o t, \quad \bar{\mathbf{F}} \equiv 0,$$
$$V(\pm 1) = V_y(\pm 1) = W(1) = 0,$$
$$\text{Poiseuille flow: } \bar{P}_x = -2/R, \quad U(\pm 1) = 0, \tag{2}$$
$$\text{Couette flow: } \bar{P}_x = 0, \quad U(-1) = 0, \quad U(1) = 1,$$

where positive parameters α and T, respectively, denote the nondimensional amplitude and period of wall oscillations. If W_w and T_w are the wall oscillation amplitude and period in physical units, then $\alpha := W_w/\bar{U} = R_w/R$ and $T := T_w/T_c$, where $R_w := W_w\delta/\nu$ is the Reynolds number defined in terms of W_w, and $T_c := \delta/\bar{U}$ is the convective time scale. The amplitude of wall oscillations is multiplied by 2 for convenience of later algebraic manipulations.

In the steady state, Eq. (1) simplifies to the x and z-direction momentum equations, which are completely decoupled

$$0 = -\bar{P}_x + (1/R)U_{yy}, \tag{3a}$$

$$W_t = (1/R)W_{yy}. \tag{3b}$$

The steady-state solution to Eqs. (2) and (3) is given by $\bar{\mathbf{u}} := [U(y)\ 0\ W(y,t)]^T$, with $U(y) = 1-y^2$ in Poiseuille flow, $U(y) = (y+1)/2$ in Couette flow, and

$$W(y,t) = 2\alpha[W_c(y)\cos\omega_o t + W_s(y)\sin\omega_o t].$$

Functions $W_c(y)$ and $W_s(y)$ represent solutions to the following system of ordinary differential equations:

$$W_s''(y) = -\Omega W_c(y), \quad W_c''(y) = \Omega W_s(y),$$
$$W_s(1) = W_c(\pm 1) = 0, \quad W_s(-1) = 1, \tag{4}$$

where $W_r''(y)$ denotes a second derivative of $W_r(y)$, that is $W_r''(y) := d^2W_r(y)/dy^2$, $r=s$ or $r=c$. Note that $\Omega := \omega_o R = \omega_w\delta^2/\nu$, with $\omega_w := 2\pi/T_w$, represents the Stokes number. It is a standard fact that the Stokes number quantifies a ratio between[19] (a) diffusive time scale $T_d := \delta^2/\nu$ and wall oscillation period T_w; (b) channel half-width δ and Stokes layer thickness $(\nu/\omega_w)^{1/2}$, $\Omega = \delta^2/(\nu/\omega_w)$. Clearly, the solution to (4) depends only on y and Ω; this dependence can be readily determined symbolically using MATHEMATICA (see Appendix A).

B. Linearized Navier-Stokes equations

The dynamics of fluctuations around a nominal flow condition $(\bar{\mathbf{u}}, \bar{P})$ are derived by expressing the flow and the forcing fields as the sum of nominal and fluctuating terms $\{\mathbf{u} := \bar{\mathbf{u}} + \mathbf{v}, P := \bar{P} + p, \mathbf{F} := \bar{\mathbf{F}} + \mathbf{d} = \mathbf{d}\}$. If $\bar{\mathbf{u}}$ represents a steady-state solution of the NS equations subject to $(\bar{P}, \bar{\mathbf{F}})$ the linearization of Eq. (1) yields

$$\mathbf{v}_t = -\boldsymbol{\nabla}_{\bar{\mathbf{u}}}\mathbf{v} - \boldsymbol{\nabla}_{\mathbf{v}}\bar{\mathbf{u}} - \boldsymbol{\nabla}p + (1/R)\Delta\mathbf{v} + \mathbf{d}, \tag{5a}$$

$$0 = \boldsymbol{\nabla}\cdot\mathbf{v}. \tag{5b}$$

These equations govern the dynamics (up to first order) of velocity and pressure fluctuations $\mathbf{v} := [u\ v\ w]^T$ and p in the presence of a body force fluctuation $\mathbf{d} := [d_1\ d_2\ d_3]^T$. This force represents an *outside excitation* to the linearized NS equations (5) and, for example, it can account for disturbances arising due to free stream turbulence or acoustic waves (which are arguably present in most flows). On the other hand, nominal velocity $\bar{\mathbf{u}}$ enters into these equations as a coefficient that multiplies velocity fluctuation vector $\mathbf{v}$. Each field in Eq. (5) is assumed to vary both temporally and spatially, e.g., $\mathbf{d} = \mathbf{d}(x,y,z,t)$.

Since the nominal velocity determines coefficients of the linearized NS equations, system (5) inherits the constant coefficients in x and z, and the *periodic coefficients in time*. Thus, the Fourier transform in x and z can be used to convert the linearized NS equations into a family of partial differential equations in y with *temporally periodic coefficients*. This family of equations is parameterized by the horizontal wavenumbers k_x and k_z, the Reynolds numbers R and R_w, and the Stokes number Ω. By applying a standard conversion to the wall-normal velocity (v)/wall-normal vorticity (η) formulation,[12] we transform Eq. (5) with $\bar{\mathbf{u}} := [U(y)\ 0\ W(y,t)]^T$ to

$$\begin{aligned}\boldsymbol{\psi}_t(k_x,y,k_z,t) &= A(k_x,k_z)\boldsymbol{\psi}(k_x,y,k_z,t)\\ &\quad + B(k_x,k_z)\mathbf{d}(k_x,y,k_z,t),\\ \mathbf{v}(k_x,y,k_z,t) &= C(k_x,k_z)\boldsymbol{\psi}(k_x,y,k_z,t),\end{aligned} \tag{6}$$

where $\boldsymbol{\psi} := [v\ \eta]^T$, and A, B, and C are given by

$$A := \begin{bmatrix} A_{11} & 0 \\ A_{21} & A_{22}\end{bmatrix}, \quad C := \frac{1}{k^2}\begin{bmatrix} ik_x\partial_y & -ik_z \\ k^2 & 0 \\ ik_z\partial_y & ik_x\end{bmatrix},$$

$$B := \begin{bmatrix} -ik_x\Delta^{-1}\partial_y & -k^2\Delta^{-1} & -ik_z\Delta^{-1}\partial_y \\ ik_z & 0 & -ik_x,\end{bmatrix},$$

$$\begin{aligned}A_{11} &:= \Delta^{-1}\left\{\frac{1}{R}\Delta^2 + ik_x[U''(y) - U(y)\Delta]\right\}\\ &\quad + ik_z\Delta^{-1}[W''(y,t) - W(y,t)\Delta],\end{aligned}$$

$$A_{21} := -ik_zU'(y) + ik_xW'(y,t),$$

$$A_{22} := (1/R)\Delta - ik_xU(y) - ik_zW(y,t),$$

$$W := \frac{2R_w}{R}\left[W_c(y)\cos\frac{\Omega t}{R} + W_s(y)\sin\frac{\Omega t}{R}\right],$$

with $i := \sqrt{-1}$ and $k^2 := k_x^2 + k_z^2$. System (6) is subject to the following boundary conditions: $\{v(k_x,\pm 1,k_z,t) = v_y(k_x,\pm 1,k_z,t) = \eta(k_x,\pm 1,k_z,t) = 0,\ \forall k_x,k_z \in \mathbb{R},\ \forall t \geq 0\}$, which are derived from the original no-slip boundary conditions on (u,v,w). Mathematical background necessary for a precise description of the above operators is given in Appendix B.

III. FREQUENCY RESPONSE OF LINEAR TIME-PERIODIC SYSTEMS

We next introduce a notion of the *frequency response* for stable linear time-periodic systems with period $T = 2\pi/\omega_o$.

It is a standard fact that a frequency response of a stable linear time-invariant system describes how a persistent harmonic input of a certain frequency propagates through the system in the steady-state. In other words, the steady-state response of a stable linear time-invariant system to an input signal of frequency ω, is a periodic signal of the same frequency, but with a modified amplitude and phase. The amplitude and phase of the output signal are precisely determined by the value of the frequency response at the input frequency ω. An in-depth discussion of the frequency response in Poiseuille and Couette flows and its utility in understanding transition is presented in Refs. 20 and 21.

On the other hand, a steady-state response of a stable linear time-periodic system to a harmonic input of frequency θ in general contains an infinite number of harmonics separated by integer multiplies of ω_o, that is $\theta + n\omega_o$. Using this fact and the analogy with the linear time-invariant systems, the frequency response of a linear time-periodic system can be defined in terms of the so-called *Bloch waves*[22] (or, equivalently, *exponentially modulated periodic* signals[23]). The latter terminology indicates that the signals of interest can be represented by a product between time periodic terms (which are decomposed into corresponding Fourier series) and an exponential term $e^{i\theta t}$ that modulates the amplitude of periodic components. Namely, the steady-state response of Eq. (6) to a Bloch wave

$$\mathbf{d}(k_x,y,k_z,t) = \sum_{n=-\infty}^{\infty}\mathbf{d}_n(k_x,y,k_z)e^{i(n\omega_o+\theta)t},$$

is also a Bloch wave

$$\mathbf{v}(k_x,y,k_z,t) = \sum_{n=-\infty}^{\infty}\mathbf{v}_n(k_x,y,k_z)e^{i(n\omega_o+\theta)t},$$

where $\mathbf{d}_n(k_x,y,k_z)$ and $\mathbf{v}_n(k_x,y,k_z)$ are the functions of y parameterized by k_x and k_z, and $\theta \in [0,\omega_o)$ is the angular frequency. The frequency response of Eq. (6) is an operator $\mathcal{H}_\theta(k_x,k_z)$ that maps a bi-infinite input vector $\mathrm{col}\{\mathbf{d}_n(k_x,y,k_z)\}_{n\in\mathbb{Z}}$ to a bi-infinite output vector $\mathrm{col}\{\mathbf{v}_n(k_x,y,k_z)\}_{n\in\mathbb{Z}}$, and it can be expressed as

$$\mathcal{H}_\theta(k_x,k_z) = \mathcal{C}(k_x,k_z)[\mathcal{E}(\theta) - \mathcal{A}(k_x,k_z)]^{-1}\mathcal{B}(k_x,k_z),$$

where $\mathcal{E}(\theta)$ is a block-diagonal operator given by $\mathcal{E}(\theta) := \mathrm{diag}\{i(\theta + n\omega_o)I\}_{n\in\mathbb{Z}}$, and I is the identity operator. On the other hand, $\mathcal{A}$, $\mathcal{B}$, and $\mathcal{C}$ represent block-Toeplitz operators (that is, operators with constant blocks along subdiagonals), e.g.,

$$\mathcal{A} := \text{toep}\{\ldots, A_2, A_1, \boxed{A_0}, A_{-1}, A_{-2}, \ldots\} = \begin{bmatrix} \ddots & \vdots & \vdots & \vdots & \iddots \\ \cdots & A_0 & A_{-1} & A_{-2} & \cdots \\ \cdots & A_1 & A_0 & A_{-1} & \cdots \\ \cdots & A_2 & A_1 & A_0 & \cdots \\ \iddots & \vdots & \vdots & \vdots & \ddots \end{bmatrix},$$

where, for notational convenience, we suppress the dependence on k_x and k_z. The box denotes the element on the main diagonal of $\mathcal{A}$. This bi-infinite matrix representation is obtained by expanding operators A, B, and C in Eq. (6) into their Fourier series, e.g., $A(k_x,k_z,t)=\Sigma_{n=-\infty}^{\infty} A_n(k_x,k_z)e^{in\omega_o t}$. Clearly, since B and C are time-invariant operators their block-Toeplitz representations simplify to block-diagonal representations, i.e.,

$$\mathcal{B}(k_x,k_z) = \text{toep}\{\ldots, 0, \boxed{B(k_x,k_z)}, 0, \ldots\} = \text{diag}\{B(k_x,k_z)\},$$

$$\mathcal{C}(k_x,k_z) = \text{toep}\{\ldots, 0, \boxed{C(k_x,k_z)}, 0, \ldots\} = \text{diag}\{C(k_x,k_z)\}.$$

The Fourier series expansion of operator $A(k_x,k_z,t)$ with $W(y,t)=2\alpha[W_c(y)\cos\omega_o t + W_s(y)\sin\omega_o t]$ is given in Appendix B 2.

For each value of (k_x,k_z,θ), $\mathcal{H}_\theta(k_x,k_z)$ is a bi-infinite matrix whose elements are one-dimensional operators in the wall-normal direction. This infinite dimensional object contains a large amount of information about the dynamical properties of system (6). In Refs. 20 and 21, the frequency responses of the NS equations in channel flows linearized around $U(y)$ were analyzed as the functions of R, k_x, and k_z. The temporal and wall-normal dynamics were aggregated by computing the $\mathcal{H}_2$ and $\mathcal{H}_\infty$ system norms.[24] At any k_x and k_z these input-output gains, respectively, quantify the variance (energy) amplification of stochastic outside disturbances and the worst case amplification of deterministic outside disturbances.[21] Since we are interested in comparing the variance amplification for channel flows with and without spanwise wall oscillations we next define the $\mathcal{H}_2$ norm for linear time-periodic system (6).

- The $\mathcal{H}_2$ norm is defined by

$$E(k_x,k_z) := \frac{1}{2\pi}\int_0^{\omega_o} \text{trace}[\mathcal{H}_\theta^*(k_x,k_z)\mathcal{H}_\theta(k_x,k_z)]d\theta. \tag{7}$$

  At any wavenumber pair, $E(k_x,k_z)$ determines the asymptotic level of variance maintained in a stable linear dynamical system subject to a stochastic outside forcing. In physics and fluid mechanics literature the $\mathcal{H}_2$ norm is also referred to as the ensemble average energy density of the statistical steady state (see, for example, Refs. 15 and 16).

We note that integration over θ in Eq. (7) can be avoided in the computation of the ensemble average energy density. Namely, the variance amplification of system (6) can be expressed in terms of a solution to the following *harmonic Lyapunov equation*:[25]

$$\mathcal{F}(k_x,k_z)\mathcal{V}(k_x,k_z) + \mathcal{V}(k_x,k_z)\mathcal{F}^*(k_x,k_z) = -\mathcal{B}(k_x,k_z)\mathcal{B}^*(k_x,k_z),$$

$$\mathcal{F}(k_x,k_z) := \mathcal{A}(k_x,k_z) - \mathcal{E}(0).$$

At any wavenumber pair (k_x,k_z), the solution to this equation is a self-adjoint block-Toeplitz operator $\mathcal{V}(k_x,k_z)$,[26]

$$\mathcal{V} := \text{toep}\{\ldots, V_2^*, V_1^*, \boxed{V_0}, V_1, V_2, \ldots\},$$

and the variance amplification is determined by

$$E(k_x,k_z) = \text{trace}[V_0(k_x,k_z)C^*(k_x,k_z)C(k_x,k_z)].$$

At any pair of the spatial wavenumbers, the entries into the harmonic Lyapunov equation are bi-infinite operator-valued (in the wall-normal direction) matrices. Thus, a discretization of the linearized NS equations in y in combination with a truncation of bi-infinite matrices would require solving a large-scale Lyapunov equation; for an accurate computation of the ensemble average energy density the entries into this equation are typically matrices with a large number of rows and columns. Since we need to determine how variance amplification changes with amplitude and frequency of the wall oscillations, as well as with the spatial wavenumbers and the Reynolds number, we are faced with a computationally intensive undertaking. In view of this, we consider a problem of the small wall oscillation amplitudes in this paper. For this special case, a perturbation analysis yields a computationally efficient method for determining the ensemble average energy density.[26] It turns out that the variance amplification can be obtained by solving a certain number of Lyapunov and Sylvester equations whose order is determined by the size of discretization in y; the number of these equations is for one greater than the highest order of perturbation parameter in the power series expansion of the ensemble average energy density.

Remark 1: The analysis of dynamical systems with inputs has a long history in circuit theory, controls, communications, and signal processing. In this analysis, it is convenient to express dynamical systems as input-output "blocks" that can be connected in a variety of cascade, series, and feedback arrangements. The utility of this approach is twofold. First, it greatly facilitates analysis and design of complex systems made up of sub-blocks that are easier to characterize. Second, it allows for modeling of dynamical inputs which are unmeasurable or uncertain. These include stochastic or deterministic uncertain signals such as noise or uncertain forcing that are inevitably present in most physical systems. An overview of how input-output analysis can be employed to uncover the mechanisms triggering early stages of transition in wall-bounded shear flows can be found in Refs. 15, 16, 20, 21, and 27.

Remark 2: The linearized NS equations in channels, pipes, and boundary-layers are characterized by non-normal dynamical generators [operator A in Eq. (6)]. An operator is normal if it has orthogonal eigenfunctions (or, equivalently, if it commutes with its adjoint).[28] It is a fact that inputs into even stable non-normal dynamical systems can be amplified by arbitrarily large factors.[29] Since the linearized NS equa-

tions in wall-bounded shear flows have non-normal generators, the spectral analysis is not capable of capturing important facets of the linearized dynamics. It turns out that in subcritical regimes the linearized NS equations experience large transient growth before eventual decay. Furthermore, these equations are exceedingly sensitive to outside disturbances or modeling uncertainties. One can arrive at these observations by performing the transient growth,[12,30,31] the pseudospectra,[28,29] or the input-output[15,16,20,21,27] analyses. The transient growth analysis reveals initial conditions that have the largest growth potential on a given time interval, the pseudospectra analysis elucidates sensitivity of the linearized NS equations to modeling errors, and the input-output analysis quantifies receptivity of the linearized dynamics to external disturbances (such as free-stream turbulence and acoustic waves). All of these methods exemplify the importance of streamwise vortices and streaks in both transitional and turbulent wall-bounded shear flows.

Remark 3: While the transient growth analysis focuses on the search for initial perturbations that gain most energy on a certain time interval, the input-output analysis is concerned with identifying the flow structures that are strongly amplified by persistent outside disturbances. Namely, in the input-output analysis the initial conditions are zero and one considers responses of the linearized dynamics to uncertain body forces. When the body forces are absent the response of stable flows eventually vanishes. However, in the presence of stochastic body forces the linearized NS equations are capable of maintaining high levels of the steady-state variance. The $\mathcal{H}_2$ norm exactly determines the asymptotic level of variance sustained in the stable linear dynamical system subject to a stochastic outside forcing.[24] Even though both transient growth and input-output analyses use a kinetic energy density of the perturbed flow field to quantify the size of velocity perturbations, there exists no general relationship between them.

Since the operators appearing in the expression for the ensemble average energy density depend on the wavenumbers k_x and k_z, the Reynolds numbers R, and R_w, and the Stokes number Ω, the variance amplification is also a function of these parameters. In Sec. IV, we provide an explicit scaling of the variance amplification with the Reynolds numbers for the streamwise constant system (6) with $R_w \ll R$, and analyze how it changes with k_z and Ω. In Sec. V, we consider the full three-dimensional perturbations in Poiseuille flow with $R=2000$, and compute the variance amplification for a value of the Stokes number that leads to the largest variance suppression for streamwise constant perturbations. All numerical computations are performed using a Matlab Differentiation Matrix Suite.[32]

IV. VARIANCE AMPLIFICATION AT $k_x=0$

In this section, we study system (6) in the important special case of streamwise constant three-dimensional perturbations. The motivation for a thorough analysis of this model stems from the fact that the streamwise constant perturbations in Poiseuille and Couette flows contribute most to the ensemble average energy density of the statistical steady state.[15,20,21,27] Our objective is to quantify the influence of small-amplitude transverse wall oscillations on the amplification of stochastic outside disturbances. We employ a perturbation analysis to provide an explicit dependence of the variance amplification on the Reynolds numbers. We also study the ensemble average energy density as a function of k_z and Ω, and identify the values of the Stokes number that lead to the variance attenuation. We show that suppression (enhancement) of turbulence by transverse wall oscillations is due to decreased (increased) levels of variance compared to the uncontrolled flow. In other words, the wall oscillation induced changes in nominal velocity constrain velocity perturbations to experience smaller (for suppression of turbulence) or larger (for enhancement of turbulence) receptivity to stochastic outside disturbances.[14]

By setting $k_x=0$ in Eq. (6) we obtain

$$\begin{aligned} \boldsymbol{\psi}_t(y,k_z,t) &= A(k_z,t)\boldsymbol{\psi}(y,k_z,t) + B(k_z)\mathbf{d}(y,k_z,t), \\ \mathbf{v}(y,k_z,t) &= C(k_z)\boldsymbol{\psi}(y,k_z,t), \end{aligned} \tag{8}$$

where, for

$$W(y,t) = \frac{2R_w}{R}\left[W_c(y)\cos\frac{\Omega t}{R} + W_s(y)\sin\frac{\Omega t}{R}\right],$$

we have (see Appendix B 2)

$$A(k_z,t) = A_0(k_z) + \frac{R_w}{R}[A_{-1}(k_z)e^{-i(\Omega/R)t} + A_1(k_z)e^{i(\Omega/R)t}],$$

with $A_{\pm 1}(k_z) := A_c(k_z) \mp iA_s(k_z)$, and

$$A_0(k_z) := \begin{bmatrix} \frac{1}{R}L_0(k_z) & 0 \\ C_{p0}(k_z) & \frac{1}{R}S_0(k_z) \end{bmatrix},$$

$$A_{\pm 1}(k_z) := \begin{bmatrix} L_{\pm 1}(k_z) & 0 \\ 0 & S_{\pm 1}(k_z) \end{bmatrix}, \quad \begin{aligned} L_{\pm 1}(k_z) &:= L_c(k_z) \mp iL_s(k_z), \\ S_{\pm 1}(k_z) &:= S_c(k_z) \mp iS_s(k_z). \end{aligned}$$

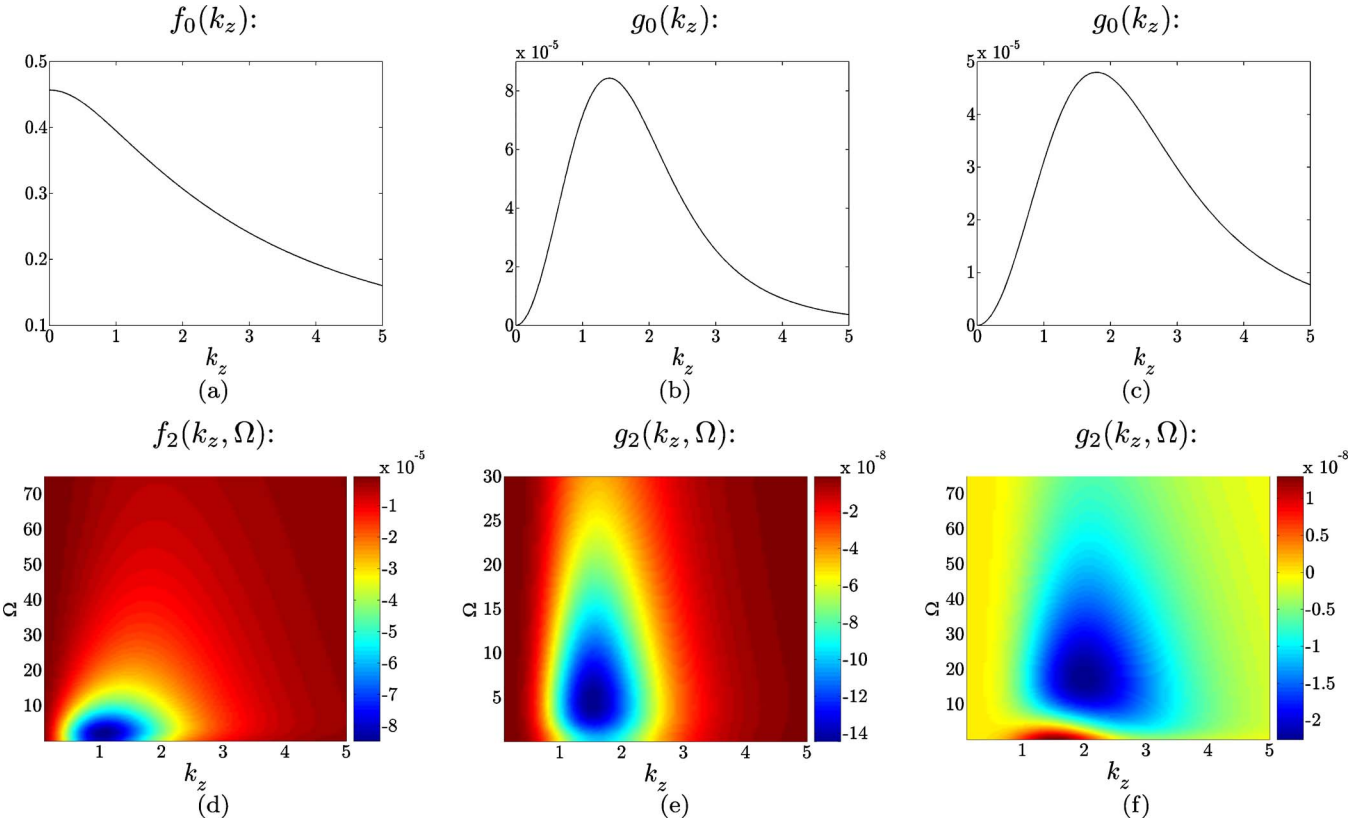

FIG. 2. (Color online) Plots of functions f_0, g_0, f_2, and g_2 in Theorem 1. The f functions are the same for all parallel channel flows $U(y)$. The terms responsible for the $O(R^3)$ variance amplification are shown in (b, e) Couette flow and (c, f) Poiseuille flow. The largest suppression of variance occurs at $\bar{\Omega}\approx 4.54$, in Couette flow, and at $\bar{\Omega}\approx 17.61$, in Poiseuille flow.

The underlying operators in $A_0(k_z)$ and $A_r(k_z)$, for $r=c$ or $r=s$, are determined by

$$L_0 := \Delta^{-1}\Delta^2, \quad C_{p0} := -ik_z U'(y),$$

$$S_0 := \Delta, \quad S_r := -ik_z W_r(y),$$

$$L_r := ik_z\Delta^{-1}[W_r''(y) - W_r(y)\Delta],$$

where $\Delta := \partial_{yy} - k_z^2$, with homogenous Dirichlet boundary conditions, and $\Delta^2 := \partial_{yyyy} - 2k_z^2\partial_{yy} + k_z^4$, with homogenous Dirichlet *and* Neumann boundary conditions. It is a standard fact that, for any (k_z, R), $A_0(k_z)$ represents a stable operator.[12] We also note that $B(k_z)B^*(k_z)=I$ and $C^*(k_z)C(k_z)=I$, which is important for the variance amplification computations (see Ref. 21 for details).

We next state the result that quantifies variance amplification of streamwise constant perturbations in parallel channel flows subject to small amplitude transverse wall oscillations.

Theorem 1: *For any parallel channel flow $U(y)$ subject to small amplitude transverse wall oscillations*

$$W(y=-1,t) = 2(R_w/R)\sin(\Omega/R)t, \quad R_w \ll R,$$

the variance amplification of streamwise constant perturbations is given by

$$E(k_z) = \left[f_0(k_z) + \sum_{n=1}^{\infty} R_w^{2n} f_{2n}(k_z,\Omega) \right] R + \left[g_0(k_z) + \sum_{n=1}^{\infty} R_w^{2n} g_{2n}(k_z,\Omega) \right] R^3.$$

Theorem 1 establishes an explicit scaling of the ensemble average energy density with the Reynolds numbers R and R_w for *any* streamwise constant parallel channel flow subject to small amplitude transverse wall oscillations. It can be shown that functions f and g in Theorem 1 represent traces of the solutions to certain operator Lyapunov equations, and the f functions do not depend on $U(y)$. Thus, $f_0(k_z)$ and $f_{2n}(k_z,\Omega)$ are the same for *all* parallel channel flows $U(y)$. On the other hand, $g_0(k_z)$ and $g_{2n}(k_z,\Omega)$ depend on the underlying parallel base flow through their dependence on the nominal shear $U'(y)$. Since a contribution of g_0 and g_{2n} to the ensemble average energy density scales as R^3, these two functions play a dominant role in the amplification of stochastic outside disturbances for the large-Reynolds-number channel flows.

In the absence of wall oscillations (that is, at $R_w=0$), we recover a formula for the ensemble average energy density of the streamwise constant NS equations linearized around $U(y)$.[27] Functions f_0 and g_0 are thoroughly analyzed in Refs. 20, 21, and 27; for completeness, they are also shown

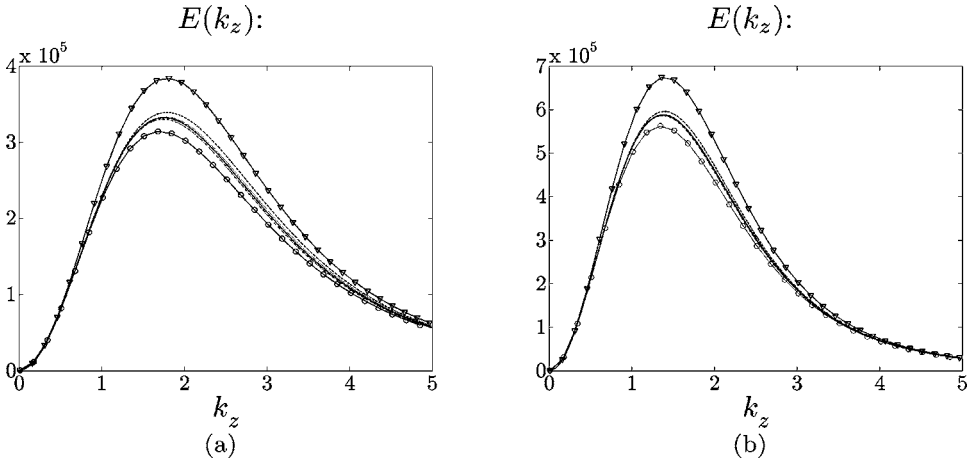

FIG. 3. The ensemble average energy densities of (a) Poiseuille flow with $\{R=2000,\ R_w=20,\ \Omega=17.61\}$, and (b) Couette flow with $\{R=2000,\ R_w=10,\ \Omega=4.54\}$. The solid curves with triangles denote uncontrolled flows; the controlled flow plots are obtained using Theorem 1 with the infinite summations approximated by the summations with: 1 (solid curves with circles), 2 (dashed curves), 3 (dot-dashed curves), 4 (dotted curves), and 5 (solid curves) terms, respectively.

in Fig. 2. The peaks in the plots of g_0 determine the most energetic structures in the velocity field excited by a broadband, stochastic input field **d**. These peaks take place at $k_z \approx 1.40$, in Couette flow, and at $k_z \approx 1.78$, in Poiseuille flow. As the plots of g_2 reveal, the Stokes number Ω determines whether transverse oscillations amplify or attenuate the most energetic components of the uncontrolled flow. We observe that the largest variance attenuation occurs at $\bar{\Omega} \approx 4.54$, in Couette flow, and at $\bar{\Omega} \approx 17.61$, in Poiseuille flow. Since the influence of f_2 on the ensemble average energy density at large Reynolds numbers is negligible compared to the influence of g_2 (R versus R^3 scaling), $\bar{\Omega}$ represents the Stokes number that provides the largest variance suppression (up to a second order in parameter R_w). Note that the largest negative contributions of g_2 to the ensemble average energy density are located in the region of spanwise wavenumbers where function g_0 peaks; this indicates that the spanwise wall oscillations introduce interactions with the most energetic modes (streamwise vortices and streaks) of the uncontrolled flow which lead to a parametric resonance.

Figures 3(a) and 3(b), respectively, show the variance amplifications of the uncontrolled Poiseuille and Couette flows with $R=2000$ (solid curves with triangles), as well as the variance amplifications of the flows subject to the wall oscillations with $\{R_w=20,\ \Omega=17.61\}$ (Poiseuille) and $\{R_w=10,\ \Omega=4.54\}$ (Couette). The variance amplification of the controlled flow is obtained using Theorem 1 by approximating the infinite summations in the expression for $E(k_z)$ by the summations with: one term (solid curves with circles), two terms (dashed curves), three terms (dot-dashed curves), four terms (dotted curves), and five terms (solid curves), respectively. Clearly, for selected values of the wall oscillation amplitudes and frequencies, the second order corrections to the ensemble average energy density give optimistic estimates of the variance suppression that can be achieved with the spanwise wall oscillations. The good news is that the curves corresponding to the sixth, eight, and tenth order corrections lie almost on the top of each other in Figs. 3(a) and 3(b). These results closely match the results obtained using large-scale computations. On the other hand, truncations with the fourth order corrections yield somewhat conservative estimates, but these estimates are much closer to the true values of the ensemble average energy density than the estimates obtained using the second order corrections.

We note that for large wall oscillation amplitudes the perturbation analysis may experience the slow rate of convergence or the lack of convergence. Despite these limitations the perturbation analysis is capable of identifying important trends in amplification of ambient disturbances. In particular, our method provides a paradigm for the optimal selection of transverse oscillation frequencies for turbulence suppression. When the frequency is selected, the large-scale computations can be used to determine the variance amplification for oscillation amplitudes at which perturbation analysis fails to converge. This is illustrated in Figs. 4(a) and 4(b), where the ensemble average energy densities of uncontrolled Poiseuille and Couette flows with $R=2000$ (solid curves), and controlled Poiseuille and Couette flows with $\{R=2000,\ R_w=20\}$ (solid curves with circles) and $\{R=2000,\ R_w=50\}$ (solid curves with triangles) are shown. In both cases the Stokes number is selected using perturbation analysis (up to a second order) which yields $\Omega=17.61$, in Poiseuille flow, and $\Omega=4.54$, in Couette flow. Thus, *properly designed* transverse wall oscillations with amplitudes equal to 2% and 5% of the maximal nominal velocity ($R_w/R=0.01$ and $R_w/R=0.025$, respectively), reduce the largest variance of the uncontrolled flows by approximately 14% and 35% in Poiseuille flow (31% and 59% in Couette flow), respectively. This demonstrates the ability of transverse wall oscillations to significantly attenuate the most energetic structures in transitional channel flows.

Flow structures that produce the most variance in Poiseuille flow with $\{R=2000,\ k_x=0,\ k_z=1.78\}$ are shown in Fig. 5. The development of the streamwise velocity perturbations in the channel's cross section (y-z plane) is given. These perturbations are streamwise independent and, as such, they do not vary in the x-direction. The parabolic shape of the uncontrolled nominal flow leads to the development of streamwise velocity in antisymmetric pairs of peaks about the channel's centerline.[30] Our results demonstrate that the properly designed transverse oscillations of the lower wall significantly weaken the intensity of streamwise streaks in the lower part of the channel. On the other hand, the dominant flow structures in the upper part of the channel remain

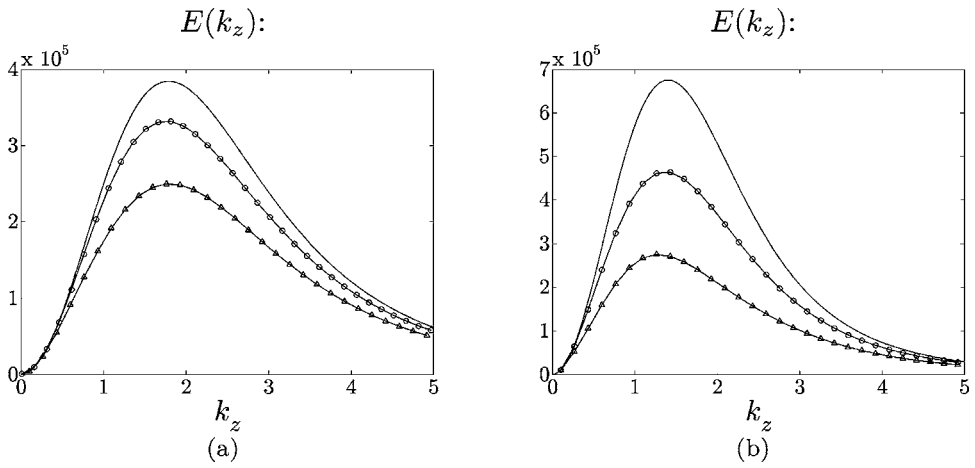

FIG. 4. (a) The ensemble average energy densities of uncontrolled Poiseuille flow with $R=2000$ (solid curve), and controlled Poiseuille flows with $\{R=2000, R_w=20, \Omega=17.61\}$ (solid curve with circles) and $\{R=2000, R_w=50, \Omega=17.61\}$ (solid curve with triangles). (b) The ensemble average energy densities of uncontrolled Couette flow with $R=2000$ (solid curve), and controlled Couette flows with $\{R=2000, R_w=20, \Omega=4.54\}$ (solid curve with circles) and $\{R=2000, R_w=50, \Omega=4.54\}$ (solid curve with triangles). Both plots are obtained by solving the large-scale truncation of the harmonic Lyapunov equation. The lower wall oscillations with amplitudes equal to 2% and 5% of the maximal nominal velocity reduce the largest variance of the uncontrolled flows by approximately 14% and 35% in Poiseuille flow (31% and 59% in Couette flow), respectively.

almost unaltered. This can be easily changed by introducing transverse oscillations of the upper wall.

The results of this section show that the transverse wall oscillations of appropriate frequency have a potential for reducing the ensemble average energy density of streamwise constant perturbation which consequently leads to a smaller turbulence production.[14,15]

V. VARIANCE AMPLIFICATION IN POISEUILLE FLOW WITH $R=2000$

In this section, we consider the full three-dimensional perturbations in Poiseuille flow with $R=2000$, and compute the ensemble average energy density for the Stokes number that leads to the largest variance suppression at $k_x=0$. As shown in Sec. IV, this value is determined by $\bar{\Omega}\approx 17.61$. The purpose of this exercise is to find out how small amplitude transverse wall oscillations of frequency $\bar{\Omega}/R$ influence ensemble average energy density of streamwise varying perturbations.

For three-dimensional perturbations we express the ensemble average energy density as

$$E(k_x,k_z) = E_0(k_x,k_z) + \sum_{n=1}^{\infty} R_w^{2n} E_{2n}(k_x,k_z),$$

and illustrate the dependence of E_0 and E_2 on (k_x,k_z) in Poiseuille flow with $\{R=2000, \Omega=17.61\}$ in Fig. 6. These plots are obtained with 150×100 grid points in the wavenumber space; they are chosen in the logarithmic scale for k_x with $\{k_{x\min}=10^{-4}, k_{x\max}=3.02\}$, and in the linear scale for k_z with $\{k_{z\min}=10^{-1}, k_{z\max}=5\}$. As the plot in Fig. 6(b) demonstrates, the small amplitude transverse oscillations reduce the variance of uncontrolled flow for wavenumbers where it

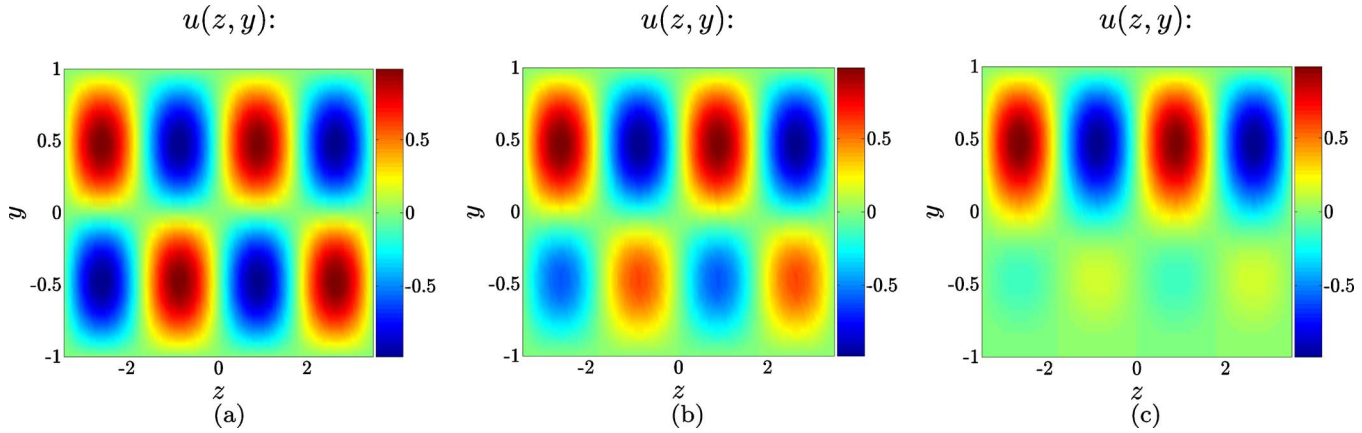

FIG. 5. (Color online) Flow structures that produce most variance in Poiseuille flow with $\{R=2000, k_x=0, k_z=1.78\}$. Plots of streamwise velocity perturbations in: (a) uncontrolled flow; (b) controlled flow with $R_w=20$ and $\Omega=17.61$; (c) controlled flow with $R_w=50$ and $\Omega=17.61$, are shown. All velocities are scaled such that their maximal values are equal to 1.

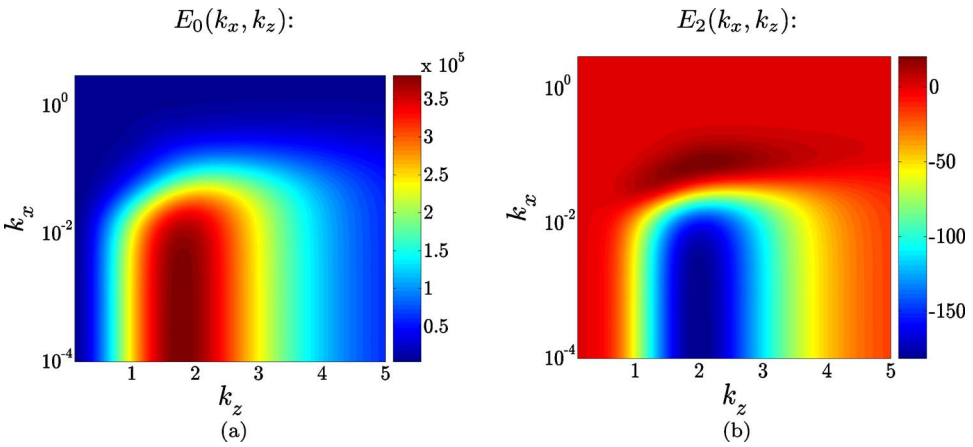

FIG. 6. (Color online) Plots of $E_0(k_x,k_z)$ and $E_2(k_x,k_z)$ in the expression for the ensemble average energy density in Poiseuille flow with $R=2000$ and $\Omega=17.61$.

achieves the largest values. This is because the regions representing large positive values of E_0 in Fig. 6(a) almost overlap with the regions representing large negative values of E_2 in Fig. 6(b). Moreover, in these regions, the higher order corrections generate alternating positive and negative contributions to the ensemble average energy density (not shown). Also, we observe that the weakly oblique perturbations create the largest positive second order (in R_w) contribution to the variance amplification. This suggests that the streamwise constant perturbations may no longer represent the most amplified flow structures at the large values of R_w. Rather, the plots of Fig. 6 open the possibility of having more complex weakly oblique dominant flow structures in channel flows subject to transverse oscillations of large amplitudes. To investigate this, we have computed the variance amplification in Poiseuille flow with $\{R=2000,\ R_w=50,\ \Omega=17.61\}$ using the large-scale truncation of the harmonic Lyapunov equation. The plot in Fig. 7 establishes that the streamwise constant structures are still most energetic. This may be attributed to the fact that the weakly oblique peaks have much smaller contributions to the higher order energy density corrections $(E_4,E_6,\ldots)$ than the streamwise constant peaks. Additionally, these weakly oblique peaks occur in the (k_x,k_z) regions where the ensemble average energy density of the uncontrolled system achieves much smaller values compared to its largest values at $k_x=0$.

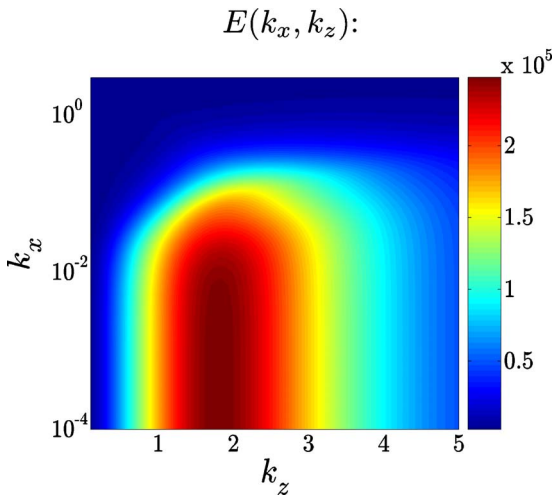

FIG. 7. (Color online) The ensemble average energy density in Poiseuille flow with $\{R=2000,\ R_w=50,\ \Omega=17.61\}$ computed using the large-scale truncation of the harmonic Lyapunov equation. A significant suppression of variance compared to the uncontrolled flow [cf. Fig. 6(a)] is observed.

The results of this section provide an additional insight about the influence of oscillation amplitude on variance amplification, and help us identify the most amplified regions in the wavenumber space for larger values of oscillation amplitudes.

VI. CONCLUDING REMARKS

This paper develops a framework for modeling and optimization of sensorless flow control strategies in wall-bounded shear flows. The new paradigm represents a spatio-temporal analog of the well-known principle of *vibrational control*, where the system's dynamical properties are altered by introducing zero-mean vibrations into the system's coefficients.[18] Depending on the relationship between the natural modes of the uncontrolled system and the forcing frequency, the vibrational control may have a potential for providing stability of the overall system and for changing its input-output norms. For example, it is well known that the inverted pendulum can be stabilized by sensorless means using high frequency oscillations of the suspension point.[18] We show that the principle of vibrational control can be also utilized in systems governing the dynamics of flow fluctuations in channel flows, where coefficients multiplying the system's state have temporal periodicity. The key observation is that there is a potential for changing dynamical properties of the linearized NS equations (in favorable or unfavorable manner) whenever temporal (or spatial) vibrations enter into the system's coefficients.

We model and analyze the influence of small amplitude transverse wall oscillations on variance amplification in channel flows. We develop models that govern the dynamics of flow fluctuations; the transverse oscillation parameters enter as coefficients, and the body force fields enter as stochastic outside disturbances into these models. We conduct a receptivity analysis for the derived models, which yields optimal oscillation frequency (as a function of the Reynolds number) for turbulence suppression. For Poiseuille and Couette flows we show that transverse wall oscillations with am-

plitudes equal to 5% of the maximal nominal velocity reduce the largest ensemble average energy density of the uncontrolled flows by approximately 35% and 59%, respectively. Our results show ability of properly designed transverse wall oscillations to reduce receptivity of the linearized NS equations to stochastic outside disturbances, which leads to decreased levels of variance in the wall-bounded shear flows.

One important aspect in evaluation of any flow control strategy is the assessment of the overall energy balance to determine whether there is any net benefit; this topic is outside the scope of the current work.

ACKNOWLEDGMENT

Financial support from the National Science Foundation under CAREER Award CMMI-06-44793 is gratefully acknowledged.

APPENDIX A: FUNCTIONS $W_s(y)$ AND $W_c(y)$

From Sec. II A, we recall that $W_c(y)$ and $W_s(y)$ represent solutions to

$$W_s''(y) = -\Omega W_c(y), \quad W_c''(y) = \Omega W_s(y),$$

$$W_s(1) = W_c(\pm 1) = 0, \quad W_s(-1) = 1.$$

This system of equations can be rewritten in terms of the following ordinary differential equation with constant coefficients,

$$q'(y) = Gq(y), \quad p(y) = Hq(y),$$

$$b = N_1 q(-1) + N_2 q(1), \quad y \in [-1,1],$$

where $p := [W_s \; W_c]^T$, $b := [1\;0\;0\;0]^T$, $q := [W_s \; W_c \; W_s' \; W_c']^T$, and

$$G := \begin{bmatrix} 0 & 0 & 1 & 0 \\ 0 & 0 & 0 & 1 \\ 0 & -\Omega & 0 & 0 \\ \Omega & 0 & 0 & 0 \end{bmatrix}, \quad H := [I_{2\times 2} \; 0_{2\times 2}],$$

$$N_1 := \begin{bmatrix} I_{2\times 2} & 0_{2\times 2} \\ 0_{2\times 2} & 0_{2\times 2} \end{bmatrix}, \quad N_2 := \begin{bmatrix} 0_{2\times 2} & 0_{2\times 2} \\ I_{2\times 2} & 0_{2\times 2}. \end{bmatrix}.$$

The solution to the above system is given by

$$p(y) = He^{G(y+1)}(N_1 + N_2 e^{2G})^{-1} b,$$

and its dependence on Ω and y can be readily determined symbolically using MATHEMATICA.

APPENDIX B: THE UNDERLYING OPERATORS

We next briefly present mathematical considerations necessary for a precise description of the operators in Eq. (6).

1. Adjoint operators

The adjoints of A, B, and C are, respectively, determined from $\langle \boldsymbol{\psi}_1, A\boldsymbol{\psi}_2 \rangle_e = \langle A^* \boldsymbol{\psi}_1, \boldsymbol{\psi}_2 \rangle_e$, $\langle \boldsymbol{\psi}, B\mathbf{d} \rangle_e = \langle B^* \boldsymbol{\psi}, \mathbf{d} \rangle$, $\langle \mathbf{v}, C\boldsymbol{\psi} \rangle = \langle C^* \mathbf{v}, \boldsymbol{\psi} \rangle_e$ (see Ref. 21 for details), where $\langle \cdot, \cdot \rangle$ denotes the standard $L^2[-1,1]$ inner product, that is

$$\langle \mathbf{v}, \mathbf{v} \rangle := \int_{-1}^{1} \mathbf{v}^* \mathbf{v} dy.$$

On the other hand, the inner product $\langle \cdot, \cdot \rangle_e$ determines the kinetic energy density of harmonic (in x and z) perturbations[30]

$$E = \langle \boldsymbol{\psi}, \boldsymbol{\psi} \rangle_e := \langle \boldsymbol{\psi}, Q\boldsymbol{\psi} \rangle,$$

$$Q := \frac{1}{k_x^2 + k_z^2} \begin{bmatrix} -\Delta & 0 \\ 0 & I \end{bmatrix}.$$

Using the above expressions, it is readily shown that $BB^* = I$, $C^*C = I$, and

$$A^* = \begin{bmatrix} A_{11}^* & A_{21}^* \\ 0 & A_{22}^*, \end{bmatrix},$$

where

$$A_{11}^* = \tfrac{1}{R}\Delta^{-1}\Delta^2 + ik_x[U(y) - \Delta^{-1}U''(y)] + ik_z[W(y,t) - \Delta^{-1}W''(y,t)],$$

$$A_{22}^* = \tfrac{1}{R}\Delta + ik_x U(y) + ik_z W(y,t),$$

$$A_{21}^* = -ik_z\Delta^{-1}U'(y) + ik_x\Delta^{-1}W'(y,t).$$

2. Fourier representation of $A(k_x, k_z, t)$

From $W(y,t) = 2\alpha[W_c(y)\cos\omega_o t + W_s(y)\sin\omega_o t]$ with $\{\alpha = R_w/R,\ \omega_o = \Omega/R\}$, and the definition of operator $A(t)$, it is clear that

$$A(t) = A_0 + 2\alpha(A_c \cos\omega_o t + A_s \sin\omega_o t) = A_0 + \frac{R_w}{R}(A_{-1}e^{-i(\Omega/R)t} + A_1 e^{i(\Omega/R)t}),$$

$$A_{\pm 1} := A_c \mp iA_s.$$

Here, A_0 denotes the system generator in Poiseuille or Couette flow, and

$$A_r := \begin{bmatrix} ik_z\Delta^{-1}(W_r''(y) - W_r(y)\Delta) & 0 \\ ik_x W_r'(y) & -ik_z W_r(y) \end{bmatrix},$$

for $r = c$ or $r = s$. Furthermore, from Appendix B 1 it follows that

$$A_r^* := \begin{bmatrix} ik_z(W_r(y) - \Delta^{-1}W_r''(y)) & ik_x\Delta^{-1}W_r'(y) \\ 0 & ik_z W_r(y) \end{bmatrix},$$

which can be used to determine $A_{\pm 1}^* = A_c^* \pm iA_s^*$. The definitions of A_0 and A_0^* are directly obtained from the definitions of $A(t)$ and $A^*(t)$ by setting $W(y,t) \equiv 0$.

[1] W. Jung, N. Mangiavacchi, and R. Akhavan, "Suppression of turbulence in wall-bounded flows by high-frequency spanwise oscillations," Phys. Fluids A **4**, 1605 (1992).
[2] A. Baron and M. Quadrio, "Turbulent drag reduction by spanwise wall oscillations," Appl. Sci. Res. **55**, 311 (1996).
[3] T. W. Berger, J. Kim, C. Lee, and J. Lim, "Turbulent boundary layer control utilizing the Lorentz force," Phys. Fluids **12**, 631 (2000).
[4] M. Quadrio and P. Ricco, "Critical assessment of turbulent drag reduction through spanwise wall oscillations," J. Fluid Mech. **521**, 251 (2004).
[5] P. Orlandi and M. Fatica, "Direct simulations of turbulent flow in a pipe

rotating about its axis," J. Fluid Mech. **343**, 43 (1997).
[6]K.-S. Choi and M. Graham, "Drag reduction of turbulent pipe flows by circular-wall oscillation," Phys. Fluids **10**, 7 (1998).
[7]M. Quadrio and S. Sibilla, "Numerical simulation of turbulent flow in a pipe oscillating around its axis," J. Fluid Mech. **424**, 217 (2000).
[8]F. Laadhari, L. Skandaji, and R. Morel, "Turbulence reduction in a boundary layer by a local spanwise oscillating surface," Phys. Fluids **6**, 3218 (1994).
[9]K.-S. Choi, J.-R. DeBisschop, and B. R. Clayton, "Turbulent boundary-layer control by means of spanwise-wall oscillation," AIAA J. **36**, 1157 (1998).
[10]K.-S. Choi, "Near-wall structure of turbulent boundary layer with spanwise-wall oscillation," Phys. Fluids **14**, 2530 (2002).
[11]P. Ricco and S. Wu, "On the effects of lateral wall oscillations on a turbulent boundary layer," Exp. Therm. Fluid Sci. **29**, 41 (2004).
[12]P. J. Schmid and D. S. Henningson, *Stability and Transition in Shear Flows* (Springer-Verlag, New York, 2001).
[13]P. J. Schmid, "Nonmodal stability theory," Annu. Rev. Fluid Mech. **39**, 129 (2007).
[14]B. F. Farrell and P. J. Ioannou, "Turbulence suppression by active control," Phys. Fluids **8**, 1257 (1996).
[15]B. F. Farrell and P. J. Ioannou, "Stochastic forcing of the linearized Navier-Stokes equations," Phys. Fluids A **5**, 2600 (1993).
[16]B. F. Farrell and P. J. Ioannou, "Variance maintained by stochastic forcing of non-normal dynamical systems associated with linearly stable flows," Phys. Rev. Lett. **72**, 1188 (1994).
[17]J. Kim, "Control of turbulent boundary layers," Phys. Fluids **15**, 1093 (2003).
[18]S. M. Meerkov, "Principle of vibrational control: theory and applications," IEEE Trans. Autom. Control **AC-25**, 755 (1980).
[19]R. L. Panton, *Incompressible Flows* (Wiley, New York, 1996).
[20]M. R. Jovanović, "Modeling, analysis, and control of spatially distributed systems," Ph.D. dissertation, University of California, Santa Barbara (2004), online, available: at http://umn.edu/home/mihailo/
[21]M. R. Jovanović and B. Bamieh, "Componentwise energy amplification in channel flows," J. Fluid Mech. **534**, 145 (2005).
[22]A. H. Nayfeh and D. T. Mook, *Nonlinear Oscillations* (Wiley, New York, 1979).
[23]N. M. Wereley and S. R. Hall, "Frequency response of linear time periodic systems," in *Proceedings of the 29th IEEE Conference on Decision and Control*, Honolulu, Hawaii, 1990, pp. 3650–3655.
[24]K. Zhou, J. C. Doyle, and K. Glover, *Robust and Optimal Control* (Prentice-Hall, New Jersey, 1996).
[25]J. Zhou, T. Hagiwara, and M. Araki, "Trace formula of linear continuous-time periodic systems via the harmonic Lyapunov equation," Int. J. Control **76**, 488 (2003).
[26]M. R. Jovanović, "$\mathcal{H}_2$ norm of linear time-periodic systems: A perturbation analysis," in *Proceedings of the 2006 American Control Conference*, Minneapolis, Minnesota (2006), pp. 1452–1457.
[27]B. Bamieh and M. Dahleh, "Energy amplification in channel flows with stochastic excitation," Phys. Fluids **13**, 3258 (2001).
[28]L. N. Trefethen and M. Embree, *Spectra and Pseudospectra: The Behavior of Non-Normal Matrices and Operators* (Princeton University Press, Princeton, 2005).
[29]L. N. Trefethen, A. E. Trefethen, S. C. Reddy, and T. A. Driscoll, "Hydrodynamic stability without eigenvalues," Science **261**, 578 (1993).
[30]K. M. Butler and B. F. Farrell, "Three-dimensional optimal perturbations in viscous shear flow," Phys. Fluids A **4**, 1637 (1992).
[31]S. C. Reddy and D. S. Henningson, "Energy growth in viscous channel flows," J. Fluid Mech. **252**, 209 (1993).
[32]J. A. C. Weideman and S. C. Reddy, "A MATLAB differentiation matrix suite," ACM Trans. Math. Softw. **26**, 465 (2000).